IEEE Access
Multidisciplinary ⋮ Rapid Review ⋮ Open Access Journal

Received 4 June 2022, accepted 20 June 2022, date of publication 23 June 2022, date of current version 5 July 2022.

Digital Object Identifier 10.1109/ACCESS.2022.3185731

RESEARCH ARTICLE

A Novel Multi-Excitation-Tooth Nonoverlapping Stator Wound Field Synchronous Machine With Salient Rotor

XIN JIANG[1], GUISHU ZHAO[1], (Member, IEEE), WEI HUA[2], (Senior Member, IEEE), SHUYE DING[1], ZHE CHANG[1], AND YAO DAI[1]

[1]School of Electrical and Automation Engineering, Nanjing Normal University, Nanjing 210046, China
[2]School of Electrical Engineering, Southeast University, Nanjing 210096, China

Corresponding author: Guishu Zhao (gzhao@njnu.edu.cn)

This work was supported in part by the Natural Science Foundation of Jiangsu Province under Grant BK20210569, in part by the Carbon Emission Peak and Neutrality Project of Jiangsu Province SBE2021100009, in part by the Natural Science Research Project of Jiangsu Higher Education Institutions under Grant 20KJB470025, and in part by the Postgraduate Research and innovation Plan Project in Jiangsu Province under Grant SJCX21_0565.

ABSTRACT In this paper, based on the conventional nonoverlapping stator wound field synchronous (N-SWFS) machine, a novel multi-excitation-tooth N-SWFS (MN-SWFS) machine is firstly proposed by changing winding configurations and the excitation-teeth shape. The electromagnetic performance of four optimized MN-SWFS machines sharing the same 12-stator-teeth but different rotor-teeth numbers, namely 12/10, 12/11, 12/13, and 12/14, is compared by finite element analysis (FEA). The corresponding simulation results show that 12/10 and 12/14 are the optimal stator-teeth/rotor-teeth combinations due to much smaller back electromotive force (back-EMF) THD and torque ripple (T_{rip}). Finally, a series of comparative studies are carried out on the proposed MN-SWFS machines and the conventional N-SWFS machines. The comparative results validate that the proposed 12/10 and 12/14 MN-SWFS machines exhibit better electromagnetic performance than the conventional 12/11 and 12/13 N-SWFS machines, such as higher fundamental back-EMF amplitude and greater torque output capability, though their cogging torque (T_{cog}) and torque ripple are slightly higher, and the torque anti-saturation ability is slightly weaker.

INDEX TERMS Stator wound field synchronous machine, nonoverlapping windings, winding configurations, multi-excitation-tooth, salient rotor, performance comparison.

I. INTRODUCTION

Permanent magnet (PM) synchronous machines have the advantages of high torque, high power, high efficiency, and easy control [1]–[6]. However, since the PMs are placed on the rotor side, high rotor temperature during high-speed operation will lead to the demagnetization of PMs, which greatly affects the reliability of the machines [7], [8]. By placing PMs on the stator side, the stator PM flux-switching (SPMFS) machines were proposed, which have a good potential for a wide range of applications owing to brushless structure, high torque and power density, good heat dissipation performance, good anti-demagnetization ability, and high reliability [9]–[12]. The uncertainty of price and supply of PMs and the requirements for magnetic field adjustment on some special occasions, such as aviation starting/power generation systems and new energy vehicles, etc., limit the use of PMs [13]–[15]. Therefore, the stator wound field flux-switching (SWFFS) machines without PMs have been extensively studied in recent years [16]–[18]. Since the SWFFS machine is a kind of stator excitation brushless machine, where the armature and excitation windings are both placed on the stator, and no PMs or windings on the rotor, the machine structure is simple, reliable, and suitable for high-speed operation [19], [20]. Also, the SWFFS machines have been proved to have the same torque output capability as SPMFS machines and good magnetic field adjustment performance [21], and they are expected to be widely used on AC speed regulation occasions.

For both SPMFS and SWFFS machines, high copper loss at high current density limits the power density and efficiency. Relevant studies [22]–[24] have shown that the copper

The associate editor coordinating the review of this manuscript and approving it for publication was Paolo Giangrande.

loss can be effectively reduced through optimization analysis, optimization design, and reasonable control methods. In addition, a large number of studies on structure optimization were carried out to further improve the electromagnetic performance of SWFFS machines. Fig. 1 shows an overlapping winding 12-stator-teeth/5-rotor-teeth (12/5) SWFFS machine, which has high output torque, but the overlapping winding structure increases the end winding length, leading to more copper loss and difficulties in the assembly and maintenance of the machine. Then, the 12/8 nonoverlapping SWFFS (N-SWFFS) machine with the segmented rotor was proposed [25], as shown in Fig. 2(a). The research shows that the nonoverlapping winding configuration can effectively simplify the stator structure and reduce copper loss. However, the segmented rotor structure increases the manufacturing cost and weakens the mechanical strength of the machine. Moreover, the segmented rotor is prone to magnetic saturation, thus decreasing the torque output capacity. Afterward, the topology of a 12/10 N-SWFFS machine was proposed by changing the segmented rotor into the salient rotor, as shown in Fig. 2(b), which has much higher mechanical strength than the segmented rotor structure. However, since the polarity of the magnetic field generated by two adjacent excitation coils is opposite, as is shown in Fig. 2(b), the excitation magnetic flux self-loop is generated, which greatly reduces the torque output capacity of the machine [26]–[28]. To further improve the output torque, the 12-stator-teeth nonoverlapping stator wound field synchronous (N-SWFS) machine

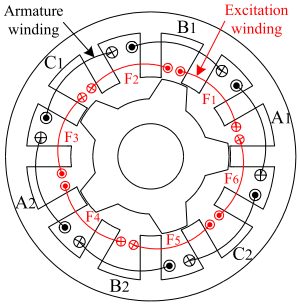

FIGURE 1. Structure and winding configuration of the 12/5 three-phase SWFFS machine.

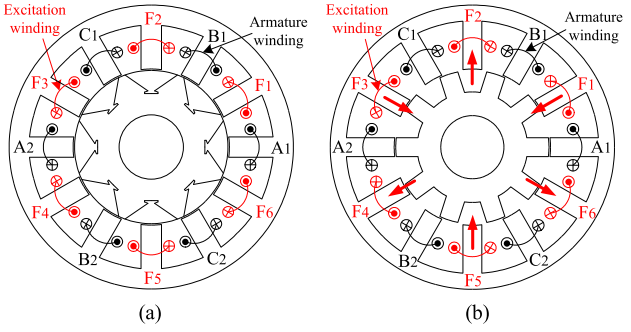

FIGURE 2. Structure and winding configuration of the three-phase N-SWFFS machines (a) 12/8 N-SWFFS machine with the segmented rotor (b) 12/10 N-SWFFS machine with the salient rotor.

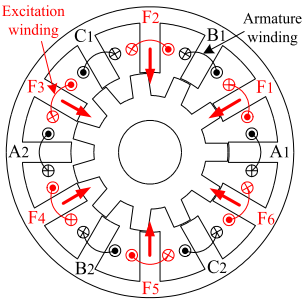

FIGURE 3. Structure and winding configuration of the 12/11 three-phase N-SWFS machine with the salient rotor.

was proposed by changing the orientation of the excitation coils to be consistent [29], as is shown in Fig. 3. And for the 12-stator-teeth N-SWFS machines, the 11- and 13-rotor-teeth structures exhibited better performance. The structure and performance comparisons of four stator wound field machines are summarized in Table 1.

TABLE 1. Comparison of the structure and performance of four stator wound field machines.

Items	SWFFSM	N-SWFFSM (Segmented rotor)	N-SWFFSM (Salient rotor)	N-SWFSM
Stator structure	complex	simple	simple	simple
Rotor structure	simple	complex	simple	simple
Torque density	highest	low	lowest	high
Mechanical strength	high	low	high	high

In this paper, in order to further improve the torque output capability of the N-SWFS machines, a novel multi-excitation-tooth N-SWFS (MN-SWFS) topology is first proposed by changing the winding configuration and the excitation-teeth shape. This paper is organized as follows. The topology formation process and the operating principle of the proposed MN-SWFS machine are explained in section II; Then, the optimal stator-teeth/rotor-teeth combinations for the proposed MN-SWFS machines are studied by finite element analysis (FEA) in section III; Afterward, a series of comparative studies between the proposed MN-SWFS machines and the conventional N-SWFS machines are carried out in section IV; Finally, some conclusions are summarized in section V.

II. MACHINE TOPOLOGY AND OPERATING PRINCIPLE

A. MACHINE TOPOLOGY

Fig. 3 presents the topology of a 12/11 three-phase N-SWFS machine, where the armature and excitation coils are alternately arranged on the stator teeth, and the layout of armature coils is "A1-B1-C1-A2-B2-C2". For the armature windings, two armature coils in radial position are connected in series to form a phase winding, such as phase winding A is composed of coils A1 and A2. The excitation winding is composed

of excitation coils F1-F6, and the magnetic flux directions generated by the excitation coils are exactly the same.

Based on the N-SWFS topology in Fig. 3, changing the winding configuration, namely two excitation coils and two armature coils being alternately arranged, a novel N-SWFS topology is formed, as is shown in Fig. 4(a), named "Model I". The layout of armature coils is "A1-A2-B1-B2-C1-C2", and the two armature coils belonging to one phase winding are separated by a mechanical angle of 90°. The polarity of the excitation magnetic flux is still the same, and the rotor is still a salient-tooth structure, which ensures the mechanical strength of the machine.

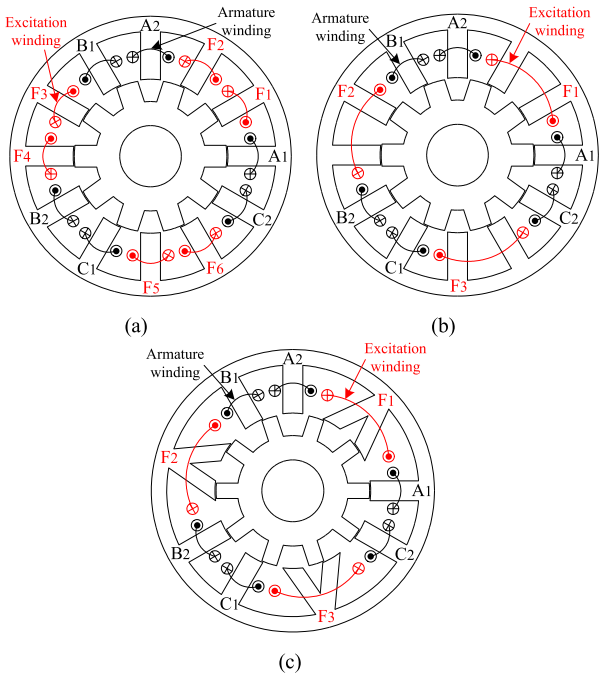

FIGURE 4. Three proposed N-SWFS machine topologies. (a) Model I (b) Model II (c) MN-SWFS machine.

However, it is not difficult to find that the effective current in the excitation slot between two adjacent excitation coils is 0 in Model I since the excitation currents of the conductors in the excitation slot are in opposite directions and equal in magnitude. Thus, the excitation slot area between the two adjacent excitation coils is ineffective.

On the basis of Model I, combining the two adjacent excitation coils into one excitation coil, namely removing the ineffective currents in the excitation slot area, the N-SWFS topology, as is shown in Fig. 4(b), is formed, named "Model II", where the excitation coils are wound across two stator teeth, and the arrangement of the armature coils remains unchanged. It can be seen that Model II has the same electromagnetic performance, smaller copper loss, and higher operating efficiency compared with Model I since the ineffective currents are removed. However, there are vacant excitation slots in this machine structure, and that is to say, the stator slot area is not fully utilized.

Changing the adjacent excitation teeth into V-shaped based on Model II, namely decreasing the useless slot area and increasing the area of the excitation slot, the novel MN-SWFS machine structure is obtained, as is presented in Fig. 4(c). The arrangement of the excitation and armature coils remains unchanged, but the excitation slot area increases, which makes full use of the space between two excitation teeth to improve the torque performance.

The MN-SWFS machine is first proposed in this paper. The operating principle, the optimal structure, and the electromagnetic performance of the MN-SWFS machine will be studied in the following sections.

B. OPERATING PRINCIPLE

Fig. 5 shows the no-load phase-A flux-linkage per turn of the proposed 12/10 MN-SWFS machine with an excitation current density of 5 A/mm^2 (J_f = 5 A/mm^2) and a slot package factor of 0.45 (k_{pf} = 0.45) at 1500 r/min. It can be seen that the flux-linkage waveforms of coil A1 and coil A2 are unipolar, and the flux-linkage waveform of winding A, namely the superposition of flux-linkage flowing in coils A1 and A2, is bipolar in an electric period.

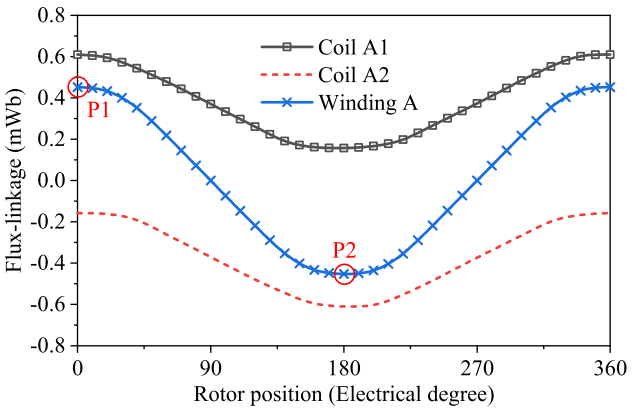

FIGURE 5. No-load phase-A flux-linkage per turn of the proposed 12/10 MN-SWFS machine with J_f = 5 A/mm^2 at 1500 r/min.

The flux-linkage distribution at the positions P1 and P2 are shown in Fig. 6, where positions P1 and P2 respectively represent the rotor position of maximum and minimum flux-linkage for phase A. At position P1, coil A1 is aligned with the rotor tooth, and coil A2 is aligned with the rotor slot, where most of the excitation magnetic fluxes flow through coil A1. Similarly, at position P2, coil A2 is aligned with the rotor tooth, and coil A1 is aligned with the rotor slot, where most of the magnetic fluxes generated by the excitation coils pass through coil A2. The excitation flux-linkage in the phase-A winding changes periodically between the maximum and minimum values, resulting in a periodically back electromotive force (back-EMF).

III. OPTIMAL STRUCTURE OF MN-SWFS MACHINE

The stator-teeth/rotor-teeth combinations have a great influence on the electromagnetic performance of stator wound

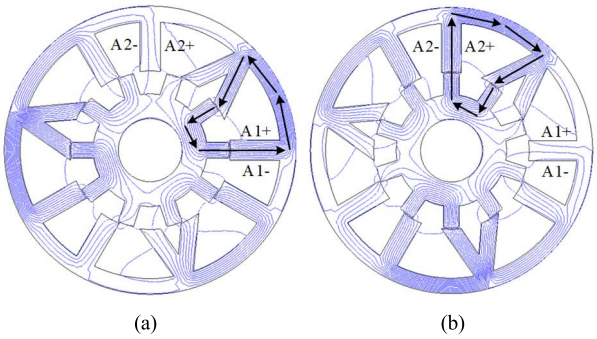

FIGURE 6. Distribution of flux lines in the 12/10 MN-SWFS machine (a) Position P1 (0 electrical degree) (b) Position P2 (180 electrical degree).

field machines. The following two principles shall be met when determining the number of rotor teeth [30].

1) The electromotive forces of the armature coils should form a three-phase armature coil phasor diagram.

2) The number of rotor teeth should be similar to the number of stator teeth for a larger winding factor and greater output torque capacity.

Therefore, in this section, the number of rotor teeth for 12-stator-teeth MN-SWFS machines is selected as 10, 11, 13, and 14 for research.

Fig. 7 shows the serial numbers of armature coils in the proposed MN-SWFS machine, where the armature coils are numbered from 1 to 6.

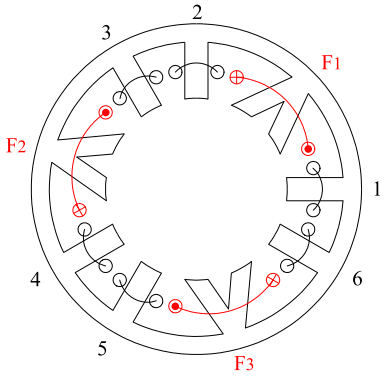

FIGURE 7. The serial number of armature coils in the proposed MN-SWFS machine.

The EMF phase of armature coils can be expressed by the following equation

$$\theta(n) = -(n-1)\theta sc(n)Pr \tag{1}$$

where n is the serial number of each armature coil; $\theta_{sc}(n)$ represents the mechanical angle between coil n and coil 1; P_r is the rotor-teeth number.

It can be seen from Fig. 7 that $\theta_{sc}(n)$ is respectively 0°, 90°, 120°, 210°, 240°, and 330°. Afterward, as shown in Fig. 8, the armature coil phasor diagram of four MN-SWFS machines with different rotor teeth numbers can be obtained. The distribution factors (k_d), pitch factors (k_p), and winding

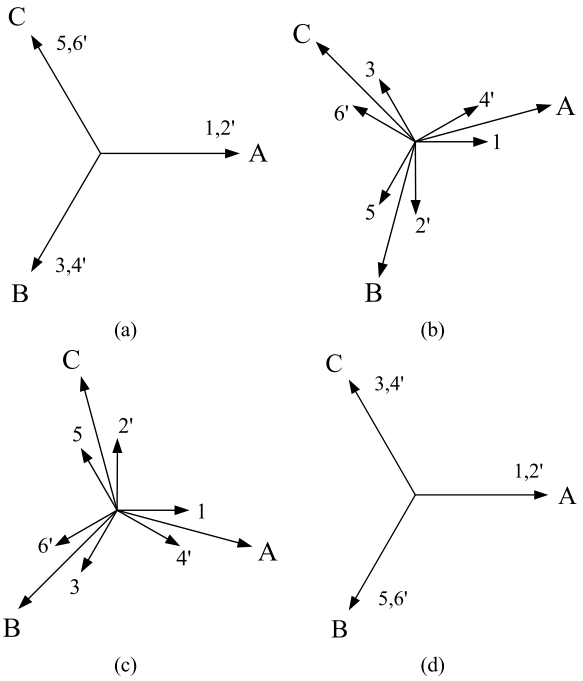

FIGURE 8. The armature coil phasor diagram of four MN-SWFS machines with different rotor teeth numbers (a) 12/10 (b) 12/11 (c) 12/13 (d) 12/14.

TABLE 2. The distribution factors, pitch factors, and winding factors of four MN-SWFS machines.

Items	12/10	12/11	12/13	12/14
k_d	1	0.966	0.966	1
k_p	0.866	0.966	0.966	0.866
k_w	0.866	0.933	0.933	0.866

factors (k_w) of the four MN-SWFS machines are listed in Table 2.

Finally, the winding configuration of four MN-SWFS machines with different rotor teeth numbers are exhibited in Fig. 9. For 12/10 and 12/14 MN-SWFS machines, the layout of the armature coils meets the form of "AABBCC", and two armature coils separated by a mechanical angle of 90° form a phase winding. While for 12/11 and 12/13 MN-SWFS machines, the layout of the armature coils meets the form of "ABCABC", and two armature coils separated by a mechanical angle of 150° form a phase winding.

In order to fairly compare the four MN-SWFS machines, the key design parameters of the four machines are multi-objective optimized for increasing average electromagnetic torque and decreasing the torque ripple by the genetic algorithm (GA) optimization combined with FEA [12], [31].

Fig. 10 presents the key design parameters of the proposed MN-SWFS machine, where the stator outer radius R_{so} (64 mm), the air-gap length g (0.5 mm), the rotor inner radius R_{ri} (14 mm), and the stack length l_a (75 mm) are fixed. Since the positions of the tip and root of stator teeth of the proposed

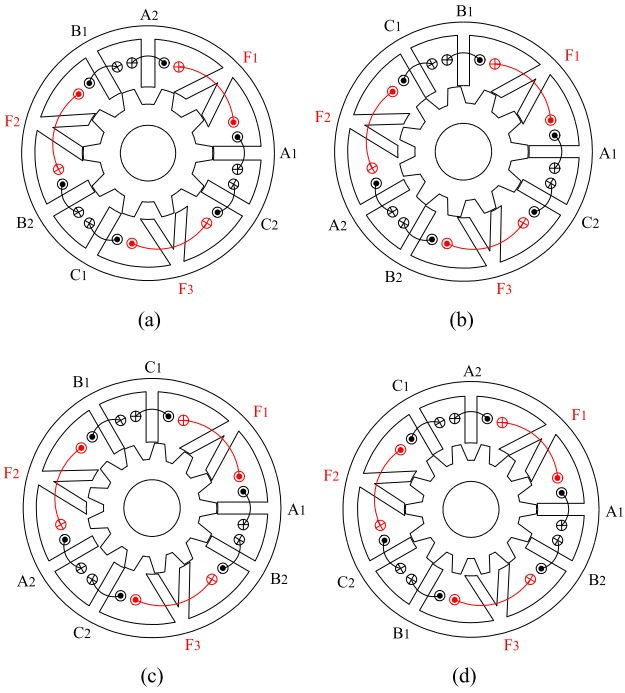

FIGURE 9. The machine topologies of four MN-SWFS machines with different rotor teeth numbers (a) 12/10 (b) 12/11 (c) 12/13 (d) 12/14.

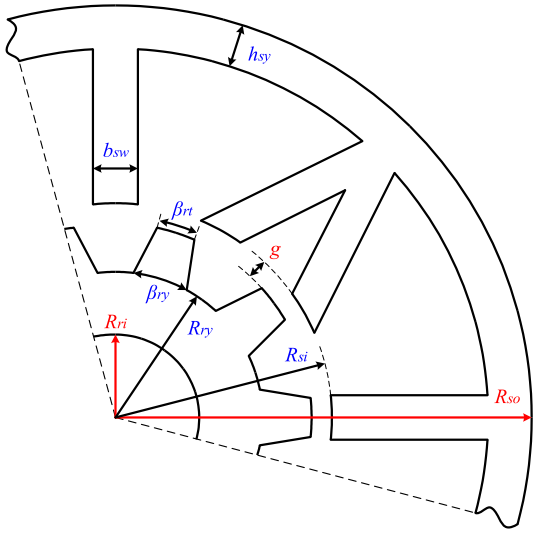

FIGURE 10. The key design parameters of the proposed MN-SWFS machine.

MN-SWFS machine are also fixed, the only parameters that need to be optimized on the stator side are the stator inner radius R_{si}, the thickness of stator yoke h_{sy}, and the width of stator teeth b_{sw}. Besides, on the rotor side, the key parameters to be optimized are the rotor yoke radius R_{ry}, the top arc of rotor teeth β_{rt}, and the bottom arc of rotor teeth β_{ry}.

The flow chart of the optimization for four MN-SWFS machines is shown in Fig. 11, where the optimization goals are the maximum average electromagnetic torque T_{avg} and

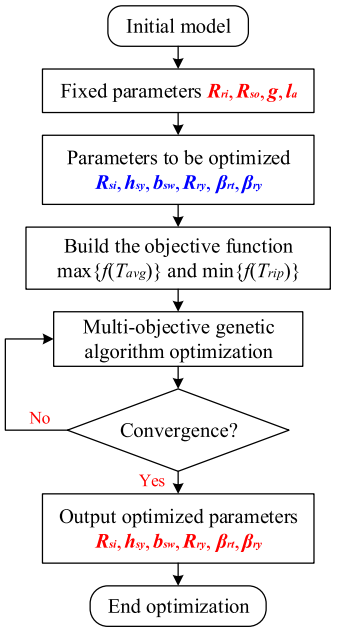

FIGURE 11. The main steps of multi-objective optimization for the proposed MN-SWFS machine.

TABLE 3. Key specifications and parameters of four 12-stator-teeth MN-SWFS machines.

Items	12/10	12/11	12/13	12/14
Stator teeth number	12			
Rotor teeth number	10	11	13	14
Stator outer radius R_{so} (mm)	64			
Stack length l_a (mm)	75			
Air-gap length g (mm)	0.5			
Stator inner radius R_{si} (mm)	33.28	32.64	32.64	33.28
Thickness of stator yoke h_{sy} (mm)	6.7	6.5	6.5	7.3
Width of Stator teeth b_{sw} (mm)	6.9	5.9	5.9	6.1
Top arc of rotor teeth β_{rt} (°)	11.5	10.5	10.5	8.0
Slot package factor (k_{pf})	0.45			
Rated speed (r/min)	1500			
Rated current density (A/mm^2)	5			
Total armature slot area (mm^2)	2412	2628	2628	2460
Total excitation slot area (mm^2)	2280	2418	2418	2262

minimum torque ripple T_{rip}. The optimized key specifications and parameters are listed in Table 3.

Based on the optimized design, the electromagnetic performance of the four MN-SWFS machines sharing the same 12-stator-teeth but with different rotor teeth numbers, namely 12/10, 12/11, 12/13, and 12/14, is compared by FEA.

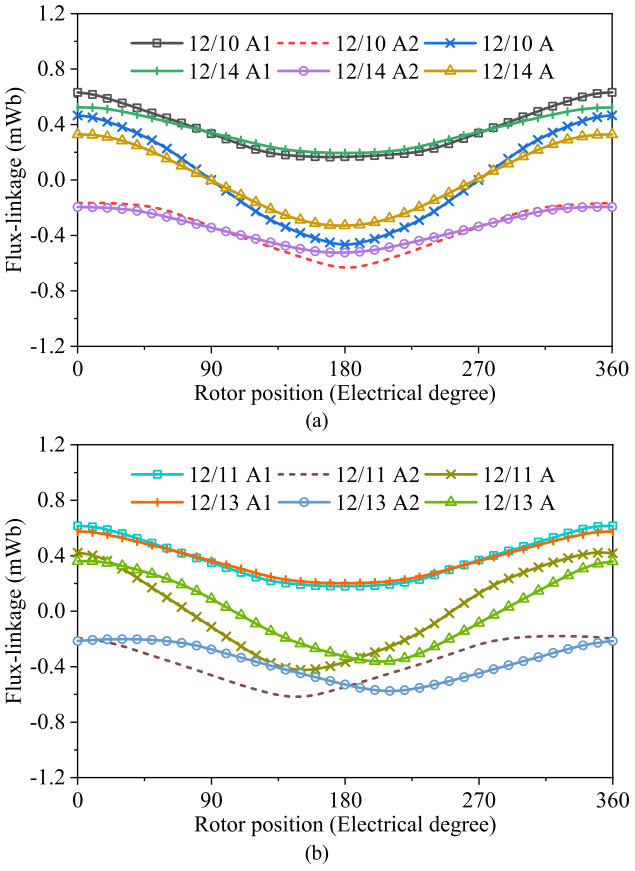

FIGURE 12. No-load phase-A flux-linkages per turn of four MN-SWFS machines at 1500 r/min (a) MN-SWFS machines with even rotor-teeth (b) MN-SWFS machines with odd rotor-teeth.

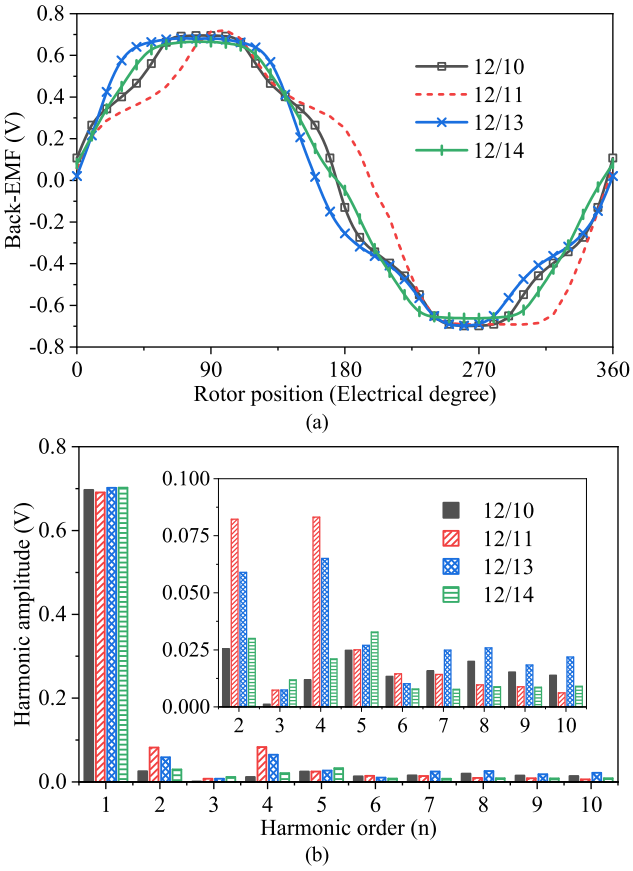

FIGURE 13. No-load phase-A back-EMFs per turn of four MN-SWFS machines at 1500 r/min (a) Waveforms (b) Harmonics.

Fig. 12 presents the no-load phase-A flux-linkages per turn of four MN-SWFS machines with the excitation current density of $J_f = 5$ A/mm^2 at 1500 r/min. It can be seen that for the even rotor-teeth structures, the flux-linkages of coils A1 and A2 have the same change trend, and the resultant phase-A flux-linkage is symmetrical in an electrical period, namely, coils A1 and A2 are complementary; For the odd rotor-teeth structures, the flux-linkage of the combined phase-A winding is asymmetrical, that is, coils A1 and A2 have no complementary. Asymmetric flux-linkage waveforms will lead to asymmetric back-EMF waveforms, higher even-order harmonics, and higher torque ripple in MN-SWFS machines, hence in the aspect of no-load flux-linkage, 12/10 and 12/14 structures have more advantages.

Fig. 13 presents the no-load phase-A back-EMFs per turn of four MN-SWFS machines at 1500 r/min, including the waveforms and harmonics. The corresponding fundamental back-EMF amplitude ($U_{m(1)}$) and the total harmonic distortion (THD) are listed in Table 4, and the THD value is calculated according to equation (2). It can be seen that the back-EMF waveforms of the 12/10 and 12/14 MN-SWFS machines are symmetrical, while the back-EMF waveforms of the 12/11 and 12/13 MN-SWFS machines are asymmetric, which are consistent with the above analysis of no-load flux-linkage. The back-EMF waveforms of the 12/10 and 12/14 MN-SWFS machines are more quasi-sinusoidal than the others, which contain lower 2nd and 4th harmonics, where the THD values are respectively 8.36% and 8.08%. For the 12/11 and 12/13 machines, the THD values are much higher, namely, 18.51% and 13.07%, respectively. Besides, the four MN-SWFS machines share similar fundamental back-EMF amplitudes, which are respectively 0.697 V, 0.691 V, 0.702 V, and 0.702 V. That is to say, under the same amplitude of fundamental back-EMF, 12/10 and 12/14 MN-SWFS machines exhibit the advantages of lower even-order harmonics and smaller THD. Hence, the optimal stator-teeth/rotor-teeth combinations for 12-stator-teeth MN-SWFS machines should be 12/10 and 12/14 from the back-EMF perspective.

$$\mathrm{THD} = \frac{\sqrt{\sum_{i=2}^{n} U_{m(i)^2}}}{U_{m(1)}} \tag{2}$$

Fig. 14 shows the electromagnetic torque waveforms of 12/10, 12/11, 12/13, and 12/14 MN-SWFS machines with $J_a = J_f = 5$ A/mm^2 under $i_d = 0$ control. The corresponding average electromagnetic torque and the torque ripple are also listed in Table 4, and the torque ripple value is calculated according to equation (3). The average electromagnetic

TABLE 4. Comparative results of four 12-stator-teeth MN-SWFS machines.

Items	12/10	12/11	12/13	12/14
$U_{m(1)}$ (V)	0.697	0.691	0.702	0.702
THD (%)	8.36	18.51	13.07	8.08
T_{avg} (Nm)	3.754	3.746	3.857	3.820
T_{rip} (%)	10.06	30.74	24.42	4.31

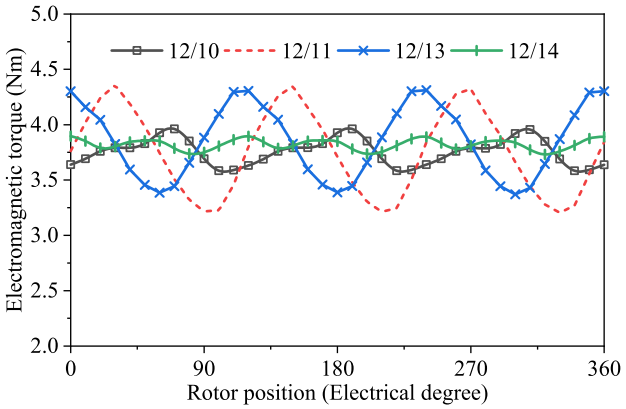

FIGURE 14. Electromagnetic torque waveforms of four MN-SWFS machines with the current density of $J_a = J_f = 5$ A/mm^2 under $i_d = 0$ control.

torque is respectively 3.754 Nm, 3.746 Nm, 3.857 Nm, and 3.820 Nm. Meanwhile, the torque ripple is respectively 10.06%, 30.74%, 24.42%, and 4.31%. Hence, it can be drawn that four MN-SWFS machines have a similar torque output capability, and the 12/10 and 12/14 MN-SWFS machines have smaller torque ripple.

$$Trip = \frac{Tmax - Tmin}{Tavg} \times 100\% \tag{3}$$

In summary, for four MN-SWFS machines, the even rotor-teeth structures have better electromagnetic performance than the odd rotor-teeth structures, that is, the 12/10 and 12/14 are the optimal combinations for the 12-stator-teeth MN-SWFS machines due to the better performance, including more quasi-sinusoidal and symmetrical back-EMFs, lower even-order harmonics, smaller THD, and smaller torque ripple.

IV. PERFORMANCE COMPARISON

According to the above analysis, for the proposed 12-stator-teeth MN-SWFS machines, 12/10 and 12/14 are the optimal structures. For the 12-stator-teeth conventional N-SWFS machines, 12/11 and 12/13 are the optimal structures. To further explore the machine performance of the proposed MN-SWFS machines, a series of comparative studies on the proposed 12/10, 12/14 MN-SWFS machines and the conventional 12/11, 12/13 N-SWFS machines, in the aspects of no-load back-EMF, cogging torque, electromagnetic torque, and torque ripple, are carried out.

A. NO-LOAD PERFORMANCE

Fig. 15(a) and (b) show the no-load back-EMF waveforms per turn of four N-SWFS machines at 1500 r/min and the harmonics after FFT decomposition, respectively. It can be seen that the 12/11 N-SWFS machine has a similar back-EMF to the 12/13 N-SWFS machine, while the 12/10 MN-SWFS machine has a similar back-EMF to the 12/14 MN-SWFS machine. The back-EMF waveforms of the four machines are all symmetrical due to the lower even-order harmonic components. In addition, the fundamental back-EMF amplitudes of 12/10 and 12/14 MN-SWFS machines are respectively 0.697 V and 0.702 V, which are much higher than that of 12/11 and 12/13 N-SWFS machines, which are respectively 0.473 V and 0.462 V. That is, the fundamental back-EMF amplitude of the proposed MN-SWFS machines is almost 50% higher than that of the conventional N-SWFS machines.

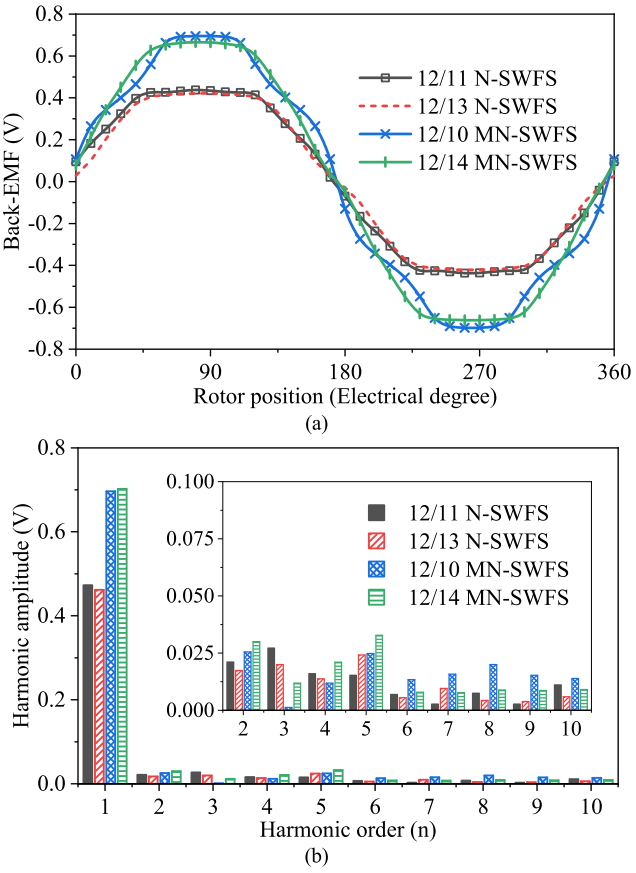

FIGURE 15. No-load phase-A back-EMFs per turn of four N-SWFS machines at 1500 r/min (a) Waveforms (b) Harmonics.

At the no-load mode, the cogging torque waveforms of four N-SWFS machines are shown in Fig. 16. The FEA results present that the peak-to-peak values of cogging torque are all not very large and are acceptable. Among them, the values of 12/11 and 12/13 N-SWFS machines are extremely small, respectively 0.061 Nm, and 0.008 Nm. While the value of the 12/14 MN-SWFS machine, namely 0.113 Nm, is slightly

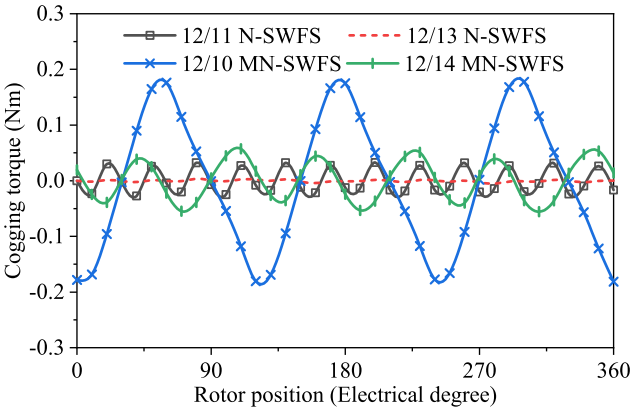

FIGURE 16. Cogging torque waveforms of four N-SWFS machines at 1500 r/min.

higher, and the value of the 12/10 MN-SWFS machine is the highest, which is 0.359 Nm.

B. TORQUE PERFORMANCE

When the excitation and armature windings of four machines are excited by a current density of 5 A/mm^2 under $i_d = 0$ control, the generated electromagnetic torque is presented in Fig. 17. The average torque of the 12/10 and 12/14 MN-SWFS machines is respectively 3.75 Nm and 3.82 Nm, which is much higher than that of the 12/11 and 12/13 N-SWFS machines, respectively 2.89 Nm and 2.81 Nm. The torque ripple of the 12/10 and 12/14 MN-SWFS and 12/11 and 12/13 N-SWFS machines is respectively 10.06%, 4.31%, 3.77%, and 1.94%. It can be seen that the average electromagnetic torque of the proposed 12/10 and 12/14 MN-SWFS machines is nearly 36% higher than those of the conventional 12/11 and 12/13 N-SWFS machines, though their torque ripple is slightly higher.

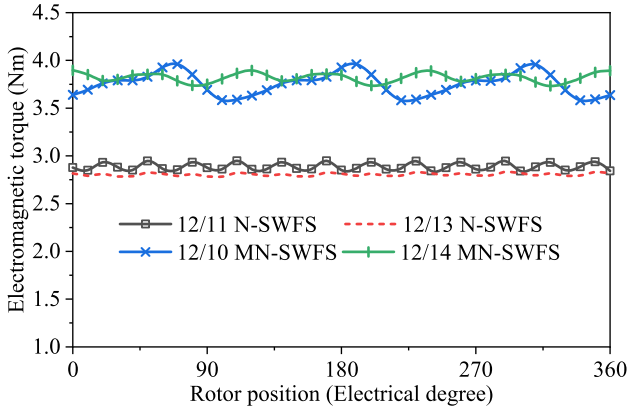

FIGURE 17. Electromagnetic torque of four N-SWFS machines with the current density of $J_a = J_f = 5$ A/mm^2 under $i_d = 0$ control.

To further compare the torque performance, the excitation and armature windings are excited by current densities varying from 1 A/mm^2 to 10 A/mm^2 under $i_d = 0$ control, and the corresponding average electromagnetic torque is shown in Fig. 18. It can be seen that the proposed two MN-SWFS machines and the conventional two N-SWFS machines have similar output torque, respectively. The torque output capability of 12/10 and 12/14 MN-SWFS machines is much larger than that of the conventional N-SWFS machines when the current density is below 8 A/mm^2, while smaller when the current density exceeds 8 A/mm^2, that is, the conventional N-SWFS machines have stronger torque anti-saturation ability.

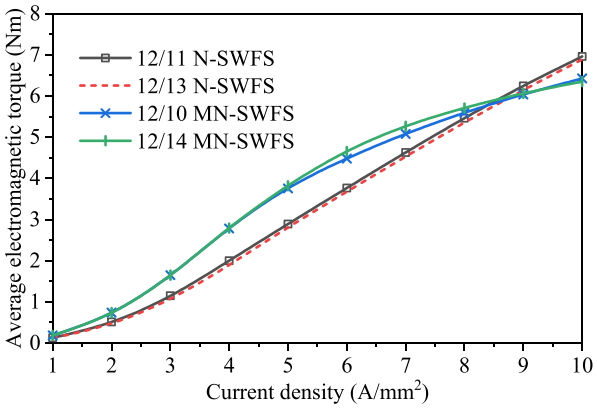

FIGURE 18. Average electromagnetic torque of four N-SWFS machines with different current densities.

In short, the 12/10 and 12/14 MN-SWFS machines exhibit better performance, including higher fundamental back-EMF amplitude and greater torque output capability when the current density is below 8 A/mm^2, although the cogging torque and torque ripple are slightly higher, and the torque anti-saturation ability is slightly weaker.

V. CONCLUSION

In this paper, based on the conventional N-SWFS machine, a novel MN-SWFS machine is first proposed by changing winding configurations and the excitation-teeth shape.

Based on the optimized design, the influence of rotor teeth numbers on the electromagnetic performance of the proposed MN-SWFS machines has been studied. It is found that 12/10 and 12/14 are the optimal stator-teeth/rotor-teeth combinations due to more quasi-sinusoidal and symmetrical back-EMFs, lower back-EMF even-order harmonics, and smaller torque ripple.

In addition, the performance of the proposed MN-SWFS machines and the conventional N-SWFS machines are quantitatively compared. The comparative results show that the fundamental back-EMF amplitudes and average torque of the proposed 12/10 and 12/14 MN-SWFS machines are respectively 50% and 36% higher than those of the conventional 12/11 and 12/13 N-SWFS machines, though their cogging torque and torque ripple are slightly higher, and the torque anti-saturation ability is slightly weaker.

REFERENCES

[1] A. M. El-Refaie, "Fractional-slot concentrated-windings synchronous permanent magnet machines: Opportunities and challenges," *IEEE Trans. Ind. Electron.*, vol. 57, no. 1, pp. 107–121, Jan. 2010.

[2] I. Petrov and J. Pyrhonen, "Performance of low-cost permanent magnet material in PM synchronous machines," *IEEE Trans. Ind. Electron.*, vol. 60, no. 6, pp. 2131–2138, Jun. 2013.
[3] W. Wang, H. Ma, X. Qiu, and J. Yang, "A calculation method for the on-load cogging torque of permanent magnet synchronous machine," *IEEE Access*, vol. 7, pp. 106316–106326, 2019.
[4] S. Wu, W. Tong, W. Li, S. Yu, and R. Tang, "Electromagnetic vibration analysis of high-speed permanent magnet synchronous machines with amorphous metal stator cores considering current harmonics," *IEEE Trans. Ind. Electron.*, vol. 67, no. 12, pp. 10156–10167, Dec. 2020.
[5] Q. Hou and S. Ding, "GPIO based super-twisting sliding mode control for PMSM," *IEEE Trans. Circuits Syst. II, Exp. Briefs*, vol. 68, no. 2, pp. 747–751, Feb. 2021.
[6] Q. Hou, S. Ding, X. Yu, and K. Mei, "A super-twisting-like fractional controller for SPMSM drive system," *IEEE Trans. Ind. Electron.*, vol. 69, no. 9, pp. 9376–9384, Sep. 2022.
[7] W. Tong, S. Wu, and R. Tang, "Research on the airflow and thermal performance in a large forced air-cooled permanent magnet synchronous machine," *IEEE Access*, vol. 7, pp. 162343–162352, 2019.
[8] C. Zhang, L. Chen, X. Wang, and R. Tang, "Loss calculation and thermal analysis for high-speed permanent magnet synchronous machines," *IEEE Access*, vol. 8, pp. 92627–92636, 2020.
[9] M. Cheng, W. Hua, J. Zhang, and W. Zhao, "Overview of stator-permanent magnet brushless machines," *IEEE Trans. Ind. Electron.*, vol. 58, no. 11, pp. 5087–5101, Nov. 2011.
[10] Y. J. Zhou and Z. Q. Zhu, "Torque density and magnet usage efficiency enhancement of sandwiched switched flux permanent magnet machines using V-shaped magnets," *IEEE Trans. Magn.*, vol. 49, no. 7, pp. 3834–3837, Jul. 2013.
[11] G. Zhao and W. Hua, "Comparative study between a novel multi-tooth and a V-shaped flux-switching permanent magnet machines," *IEEE Trans. Magn.*, vol. 55, no. 7, pp. 1–8, Jul. 2019.
[12] X. Zhu, D. Fan, L. Mo, Y. Chen, and L. Quan, "Multiobjective optimization design of a double-rotor flux-switching permanent magnet machine considering multimode operation," *IEEE Trans. Ind. Electron.*, vol. 66, no. 1, pp. 641–653, Jan. 2019.
[13] E. F. Farahani, M. A. J. Kondelaji, and M. Mirsalim, "An innovative hybrid-excited multi-tooth switched reluctance motor for torque enhancement," *IEEE Trans. Ind. Electron.*, vol. 68, no. 2, pp. 982–992, Feb. 2021.
[14] B. Gaussens, E. Hoang, M. Lecrivain, P. Manfe, and M. Gabsi, "A hybrid-excited flux-switching machine for high-speed DC-alternator applications," *IEEE Trans. Ind. Electron.*, vol. 61, no. 6, pp. 2976–2989, Jun. 2014.
[15] A. Nasr, S. Hlioui, M. Gabsi, M. Mairie, and D. Lalevee, "Design optimization of a hybrid-excited flux-switching machine for aircraft-safe DC power generation using a diode bridge rectifier," *IEEE Trans. Ind. Electron.*, vol. 64, no. 12, pp. 9896–9904, Dec. 2017.
[16] J. T. Chen, Z. Q. Zhu, S. Iwasaki, and R. Deodhar, "Low cost flux-switching brushless AC machines," in *Proc. IEEE Vehicle Power Propuls. Conf.*, Lille, France, Sep. 2010, pp. 1–6.
[17] Z. Q. Zhu, Z. Z. Wu, D. J. Evans, and W. Q. Chu, "A wound field switched flux machine with field and armature windings separately wound in double stators," *IEEE Trans. Energy Convers.*, vol. 30, no. 2, pp. 772–783, Jun. 2015.
[18] Z. Z. Wu, Z. Q. Zhu, C. Wang, J. C. Mipo, S. Personnaz, and P. Farah, "Reduction of open-circuit DC-winding-induced voltage in wound field switched flux machines by skewing," *IEEE Trans. Ind. Electron.*, vol. 66, no. 3, pp. 1715–1726, Mar. 2019.
[19] Y. J. Zhou and Z. Q. Zhu, "Comparison of low-cost single-phase wound-field switched-flux machines," *IEEE Trans. Ind. Appl.*, vol. 50, no. 5, pp. 3335–3345, Sep. 2014.
[20] G. Zhao, W. Hua, and J. Qi, "Comparative study of wound-field flux-switching machines and switched reluctance machines," *IEEE Trans. Ind. Appl.*, vol. 55, no. 3, pp. 2581–2591, May 2019.
[21] Y. Tang, J. J. H. Paulides, T. E. Motoasca, and E. A. Lomonova, "Flux-switching machine with DC excitation," *IEEE Trans. Magn.*, vol. 48, no. 11, pp. 3583–3586, Nov. 2012.
[22] W. Yu, W. Hua, P. Wang, and W. Xia, "Comparative analysis of AC loss with round copper wire and flat copper wire of high-speed stator PM flux-switching machine: Comparative analysis of AC loss of HS-SPMFS machine," in *Proc. IEEE 4th Int. Electr. Energy Conf. (CIEEC)*, Wuhan, China, May 2021, pp. 1–5.
[23] Y. Liang, F. Zhao, K. Xu, W. Wang, J. Liu, and P. Yang, "Analysis of copper loss of permanent magnet synchronous motor with formed transposition winding," *IEEE Access*, vol. 9, pp. 101105–101114, 2021.
[24] W. Ding and S. Li, "Maximum ratio of torque to copper loss control for hybrid excited flux-switching machine in whole speed range," *IEEE Trans. Ind. Electron.*, vol. 66, no. 2, pp. 932–943, Feb. 2019.
[25] A. Zulu, B. C. Mecrow, and M. Armstrong, "A wound-field three-phase flux-switching synchronous motor with all excitation sources on the stator," *IEEE Trans. Ind. Appl.*, vol. 46, no. 6, pp. 2363–2371, Nov./Dec. 2010.
[26] F. Khan, E. Sulaiman, and M. F. Omar, "Design and characteristic investigations of 12Slot-8Pole and 12Slot-10Pole wound field three-phase switched-flux machines," in *Proc. 3rd IET Int. Conf. Clean Energy Technol. (CEAT)*, Kuching, Malaysia, 2014, pp. 1–5.
[27] F. Khan, E. Sulaiman, and M. Z. Ahmad, "Coil test analysis of wound-field three-phase flux switching machine with non-overlapping winding and salient rotor," in *Proc. IEEE 8th Int. Power Eng. Optim. Conf. (PEOCO)*, Langkawi, Malaysia, Mar. 2014, pp. 243–247.
[28] E. Sulaiman, F. Khan, M. F. Omar, G. M. Romalan, and M. Jenal, "Optimal design of wound-field flux switching machines for an all-electric boat," in *Proc. 22nd Int. Conf. Electr. Mach. (ICEM)*, Lausanne, Switzerland, Sep. 2016, pp. 2464–2470.
[29] Z. Q. Zhu, Y. J. Zhou, and J. T. Chen, "Electromagnetic performance of nonoverlapping stator wound field synchronous machine with salient pole rotor," *IEEE Trans. Magn.*, vol. 51, no. 11, pp. 1–4, Nov. 2015.
[30] W. Jiang, W. Huang, X. Lin, Y. Zhao, and S. Zhu, "Analysis of rotor poles and armature winding configurations combinations of wound field flux switching machines," *IEEE Trans. Ind. Electron.*, vol. 68, no. 9, pp. 7838–7849, Sep. 2021.
[31] X. Li, F. Shen, S. Yu, and Z. Xue, "Flux-regulation principle and performance analysis of a novel axial partitioned stator hybrid-excitation flux-switching machine using parallel magnetic circuit," *IEEE Trans. Ind. Electron.*, vol. 68, no. 8, pp. 6560–6573, Aug. 2021.

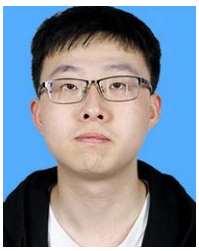

XIN JIANG was born in Changzhou, Jiangsu, China, in 1997. He received the B.S. degree in process equipment and control engineering from the Hebei University of Technology, in 2020. He is currently pursuing the degree with the Electrical Engineering Department, School of Electrical and Automation, Nanjing Normal University. His research interest includes design and optimization of stator-excited brushless machines.

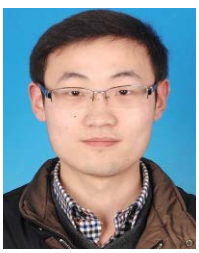

GUISHU ZHAO (Member, IEEE) received the B.S. degree in electrical engineering from the Wuhan University of Technology, Wuhan, China, in 2012, and the Ph.D. degree in electrical engineering from Southeast University, Nanjing, China, in 2019.

Since 2019, he has been with Nanjing Normal University, where he is currently a Lecturer with the School of Electrical and Automation Engineering. His current research interest includes design and control of stator-excited brushless machines.

WEI HUA (Senior Member, IEEE) received the B.Sc. and Ph.D. degrees in electrical engineering from Southeast University, Nanjing, China, in 2001 and 2007, respectively. From 2004 to 2005, he was with the Department of Electronics and Electrical Engineering, The University of Sheffield, Sheffield, U.K., as a Joint-Supervised Ph.D. Student. Since 2007, he has been with Southeast University, where he is currently a Chief Professor, and a Distinguished Professor of Jiangsu Province. Since 2010, he has been working with the Yancheng Institute of New Energy Vehicles, Southeast University. He has coauthored more than 150 technical articles. He holds 50 patents in his areas of interest. His research interests include design, analysis, and control of electrical machines, especially for PM brushless machines and switching reluctance machines.

SHUYE DING was born in 1978. He received the B.S., M.S., and Ph.D. degrees in electrical machinery and appliance from the Harbin University of Science and Technology, Harbin, China, in 2001, 2004, and 2008, respectively.

He is currently a Professor with the School of Electrical and Automation Engineering, Nanjing Normal University, Nanjing, China. He is the author or coauthor of more than 80 published peer-reviewed articles and holds more than ten patents. His research interests include synthesis physical fields of large electrical machines and theoretical study of special electrical machines.

ZHE CHANG was born in Luoyang, Henan, China, in 1998. He received the B.S. degree in electrical engineering and automation from Henan Polytechnic University, in 2020. He is currently pursuing the degree with the Electrical Engineering Department, School of Electrical and Automation, Nanjing Normal University. His research interest includes design and optimization of stator-excited brushless machines.

YAO DAI was born in Yancheng, Jiangsu, China, in 1996. She received the B.S. degree in electrical engineering from Southeast University Chengxian College, in 2019. She is currently pursuing the degree with the Electrical Engineering Department, School of Electrical and Automation, Nanjing Normal University. Her research interest includes design and optimization of mutually coupled switched reluctance machines.